Physics Letters B 750 (2015) 252–258

Contents lists available at ScienceDirect

Physics Letters B

www.elsevier.com/locate/physletb

Threshold π^0 photoproduction on transverse polarised protons at MAMI

A2 Collaboration at MAMI

S. Schumann [a,b], P.B. Otte [a], C.S. Akondi [c], J.R.M. Annand [d], H.-J. Arends [a], R. Beck [e], A.M. Bernstein [b], N. Borisov [f], A. Braghieri [g], W.J. Briscoe [i], S. Cherepnya [j], C. Collicott [k], S. Costanza [g,h], E.J. Downie [a,i], M. Dieterle [l], C. Fernández-Ramírez [m], A. Fix [n], L.V. Fil'kov [j], S. Garni [l], D.I. Glazier [o,d], W. Gradl [a], G. Gurevich [p], P. Hall-Barrientos [o], D. Hamilton [d], D. Hornidge [q], D. Howdle [d], G.M. Huber [r], V.L. Kashevarov [a,j], I. Keshelashvili [l], R. Kondratiev [p], M. Korolija [s], B. Krusche [l], A. Lazarev [f], V. Lisin [p], K. Livingston [d], I.J.D. MacGregor [d], J. Mancel [d], D.M. Manley [c], P.P. Martel [t,b], E.F. McNicoll [d], W. Meyer [u], D. Middleton [q,a], R. Miskimen [t], A. Mushkarenkov [g,t], B.M.K. Nefkens [v,1], A. Neganov [f], A. Nikolaev [e], M. Oberle [l], M. Ostrick [a,*], H. Ortega [a], P. Ott [a], B. Oussena [a], D. Paudyal [r], P. Pedroni [g], A. Polonski [p], V.V. Polyanski [j], S. Prakhov [v], G. Reicherz [u], T. Rostomyan [l], A. Sarty [k], M.H. Sikora [o], V. Sokhoyan [a,i], O. Steffen [a], I.I. Strakovsky [i], Th. Strub [l], I. Supek [s], L. Tiator [a], A. Thomas [a], M. Unverzagt [a], Yu.A. Usov [f], D.P. Watts [o], D. Werthmüller [d,l], L. Witthauer [l], M. Wolfes [a]

[a] *Institut für Kernphysik, Johannes Gutenberg-Universität Mainz, 55099 Mainz, Germany*
[b] *Massachusetts Institute of Technology, Cambridge, MA 02139-4307, USA*
[c] *Kent State University, Kent, OH 44242-0001, USA*
[d] *SUPA School of Physics and Astronomy, University of Glasgow, Glasgow G12 8QQ, United Kingdom*
[e] *Helmholtz-Institut für Strahlen- und Kernphysik, Universität Bonn, 53115 Bonn, Germany*
[f] *Joint Institute for Nuclear Research, 141980 Dubna, Russia*
[g] *INFN Sezione di Pavia, 27100 Pavia PV, Italy*
[h] *Dipartimento di Fisica, Università di Pavia, 27100 Pavia PV, Italy*
[i] *The George Washington University, Washington, DC 20052-0001, USA*
[j] *Lebedev Physical Institute, 119991 Moscow, Russia*
[k] *Department of Astronomy and Physics, Saint Mary's University, Halifax, Nova Scotia B3H 3C3, Canada*
[l] *Departement für Physik, Universität Basel, 4056 Basel, Switzerland*
[m] *Jefferson Lab, Newport News, VA 23606, USA*
[n] *Laboratory of Mathematical Physics, Tomsk Polytechnic University, 634034 Tomsk, Russia*
[o] *SUPA School of Physics, University of Edinburgh, Edinburgh EH9 3JZ, United Kingdom*
[p] *Institute for Nuclear Research, 125047 Moscow, Russia*
[q] *Mount Allison University, Sackville, New Brunswick E4L 1E6, Canada*
[r] *University of Regina, Regina, Saskatchewan S4S 0A2, Canada*
[s] *Rudjer Boskovic Institute, HR-10000 Zagreb, Croatia*
[t] *University of Massachusetts, Amherst, MA 01003, USA*
[u] *Institut für Experimentalphysik, Ruhr-Universität, 44780 Bochum, Germany*
[v] *University of California Los Angeles, Los Angeles, CA 90095-1547, USA*

* Corresponding author.
E-mail address: ostrick@kph.uni-mainz.de (M. Ostrick).

http://dx.doi.org/10.1016/j.physletb.2015.09.015

ARTICLE INFO

Article history:
Received 29 April 2015
Received in revised form 5 August 2015
Accepted 7 September 2015
Available online 14 September 2015
Editor: V. Metag

Keywords:
Threshold π^0 photoproduction
Target asymmetry
Electromagnetic multipoles

ABSTRACT

Polarisation-dependent differential cross sections σ_T associated with the target asymmetry T have been measured for the reaction $\gamma\vec{p} \to p\pi^0$ with transverse target polarisation from π^0 threshold to photon energies of 190 MeV. The data were obtained using a frozen-spin butanol target with the Crystal Ball / TAPS detector set-up and the Glasgow photon tagging system at the Mainz Microtron MAMI. Results for σ_T have been used in combination with our previous measurements of the unpolarised cross section σ_0 and the beam asymmetry Σ for a model-independent determination of S- and P-wave multipoles in the π^0 threshold region, which includes for the first time a direct determination of the imaginary part of the E_{0+} multipole.

1. Introduction

Recent accurate threshold π^0 photoproduction [1] and pionic H and D atom experiments [2,3] have supported the concept that low-energy πN dynamics reflect the spontaneous chiral symmetry breaking in QCD and the quasi Nambu–Goldstone boson nature of the pion [4–6]. This conclusion is based on the agreement of Chiral Perturbation Theory (ChPT) calculations [4,5] with the data for pion photoproduction [7–11] and pionic atoms [12]. These calculations are based on the fact that Nambu–Goldstone bosons interact weakly with other hadrons at low energies where the S-wave production and interactions go to zero in the chiral limit of vanishing up and down quark masses. The near-threshold interactions are important to measure since they are an explicit effect of chiral symmetry breaking and have been calculated by ChPT. Isospin breaking caused by both electromagnetic interactions and the mass difference of the up and down quarks [13–15] has to be taken into account to extract consistent pion-nucleon scattering lengths from pionic H and D [12].

Despite many successes, not all of the chiral predictions have been fully tested. For pion photoproduction reactions, the required measurements involve polarisation observables and small cross sections, which have presented longstanding technical challenges [16]. The A2 Collaboration at Mainz has met these challenges by deploying an almost 4π detector, tagged linear and circular polarised photon beams, and polarised targets. With our past measurement of the $\vec{\gamma}p \to \pi^0 p$ reaction [1] using linear polarised photons and an unpolarised liquid H_2 target we have provided the first assessment of the energy range where ChPT can be applied to this reaction [1,7–9]. These are first steps towards an accurate measurement of the energy dependence of the pion photoproduction multipoles.

In this Letter, we present the first results in the near-threshold region for the $\gamma\vec{p} \to \pi^0 p$ transverse polarised target cross section $\sigma_T = \sigma_0 T$, where T is the polarised target asymmetry and σ_0 is the unpolarised differential cross section [16]. The target asymmetry T is a time-reversal-odd observable [17–19] that is sensitive to $\mathrm{Im}\left[\mathcal{M}_1^* \mathcal{M}_2\right]$. Therefore σ_T gives access to the imaginary part of the E_{0+} multipole for π^0 photoproduction, which is sensitive to the πN phase shifts through the Fermi–Watson theorem [20,21]. Isospin breaking leads to a slightly higher threshold for $n\pi^+$, which produces a unitary cusp in the E_{0+} multipole for $\gamma p \to p\pi^0$. This cusp causes a rapid rise in the imaginary part of $\mathrm{Im}E_{0+}$ for photon energies ω just above the $\gamma p \to n\pi^+$ reaction threshold [22,23], which has been directly observed for the first time in this experiment. In this energy region the imaginary part of E_{0+} can be parametrised as [22]

$$\mathrm{Im}E_{0+} = \beta(\omega)\frac{q_{\pi^+}}{m_{\pi^+}} \tag{1}$$

with the π^+ momentum q_{π^+} and mass m_{π^+}. The parameter $\beta(\omega)$ is given by unitarity from

$$\beta(\omega) = \mathrm{Re}E_{0+}(n\pi^+) \cdot f_{\mathrm{cex}}(n\pi^+ \to p\pi^0) \cdot m_{\pi^+} \tag{2}$$

with the $\gamma p \to n\pi^+$ multipole $E_{0+}(n\pi^+)$ and the charge-exchange amplitude $f_{\mathrm{cex}}(n\pi^+ \to p\pi^0)$ for the $n\pi^+ \to p\pi^0$ reaction at the same centre-of-mass energy [22,23]. At the $n\pi^+$ threshold ($\omega_{\mathrm{thr}} =$ 151.44 MeV) this relation transforms to

$$\beta(\omega_{\mathrm{thr}}) = \mathrm{Re}E_{0+}(n\pi^+) \cdot a_{\mathrm{cex}}(n\pi^+ \to p\pi^0) \cdot m_{\pi^+} \tag{3}$$

where $a_{\mathrm{cex}}(n\pi^+ \to p\pi^0)$ is the charge-exchange scattering length [22,23]. The most accurate value for $a_{\mathrm{cex}}(n\pi^+ \to p\pi^0) = (0.1195 \pm 0.0016)/m_{\pi^+}$ comes from an analysis of pionic H and D data [2,3] combined with ChPT calculations including isospin breaking due to electromagnetic interactions and the mass difference of the up and down quarks [12]. Together with the latest determination of $\mathrm{Re}E_{0+}(n\pi^+) = (28.06 \pm 0.27_{\mathrm{stat}} \pm 0.45_{\mathrm{syst}}) \cdot 10^{-3}/m_{\pi^+}$ from Ref. [24], which is good agreement with the predictions of ChPT [25], one obtains a value of $\beta(\omega_{\mathrm{thr}}) = (3.35 \pm 0.08) \cdot 10^{-3}/m_{\pi^+}$ where statistical and systematic uncertainties have been added in quadrature. At higher energies $\omega > \omega_{\mathrm{thr}}$ unitarity requires that $\beta(\omega)$ decreases in magnitude since both $\mathrm{Re}E_{0+}(\gamma p \to n\pi^+)$ and $f_{\mathrm{cex}}(\pi^+ n \to \pi^0 p)$ decrease in magnitude with increasing energy. However the magnitude of the decrease is model dependent so it cannot be completely specified by unitarity.

2. Experimental set-up

The reaction $\gamma\vec{p} \to p\pi^0$ on a transverse polarised target has been measured at the Mainz Microtron (MAMI) electron accelerator facility [26] using the Glasgow tagging spectrometer [27,28] and the Crystal Ball / TAPS detector set-up. Bremsstrahlung photons are produced by scattering a 450 MeV electron beam on a 10 µm thick copper radiator. Scattered electrons are separated from the main beam by a large-acceptance magnetic dipole spectrometer and their energy E_e is determined by an array of detectors placed in the focal plane. Therefore the energy of the emitted photon is given by $\omega = E_0 - E_e$, where E_0 is the known electron beam energy. The resulting energy-tagged photon beam covers an energy range from 125 to 420 MeV at an average energy resolution of $\Delta\omega \simeq 1.2$ MeV and a tagged photon flux of $0.6 \cdot 10^7$ s^{-1}. The systematic uncertainty of the tagger energy calibration is $\delta\omega =$ 0.5 MeV. The photon flux is determined by counting the scattered electrons and correcting for the loss of photons due to collimation. This loss is periodically measured by a total-absorption lead glass counter, which is moved into the photon beam line. At reduced beam intensity the lead glass detector is able to directly

[1] Deceased.

measure the collimated photon flux Φ_γ, which is compared to the rate of scattered electrons Φ_e. With a 2.5 mm diameter collimator, the tagging efficiency Φ_γ/Φ_e is approximately 10%. Transverse polarised target protons are provided by a frozen-spin butanol (C_4H_9OH) target [29] equipped with a four-layer saddle coil, which provides a 0.45 T holding field oriented perpendicular to the beam axis [30]. The target container has a length of 2 cm and a diameter of 2 cm and is filled with 2 mm diameter TEMPO-doped butanol beads at a packing fraction of 61% [31]. The resulting free-proton area-density is $9.27 \cdot 10^{22}$ cm^{-2}. A ^{3}He/^{4}He dilution refrigerator keeps the target material at temperatures around 25 mK, which provides relaxation times of about 1500 h. The target polarisation is measured at the beginning and the end of each data-taking period and the average proton polarisation has been determined to be 79%. The direction of the target polarisation vector was regularly reversed during the experiment to reduce systematic uncertainties. The $p\pi^0$ final state was measured with the Crystal Ball (CB) as the central photon spectrometer and TAPS as a forward detector system. The Crystal Ball consists of 672 NaI(Tl) crystals and covers the full azimuthal range and a polar angle range from 20° to 160°, corresponding to a solid angle coverage of 93% of 4π. A cylindrical barrel of 24 plastic scintillators surrounding the target and aligned parallel to the beam axis is used to distinguish charged and neutral particles. Polar angles between 4° and 20° are covered by the TAPS detector [32,33] with 366 BaF_2 modules and 72 $PbWO_4$ crystals arranged as a hexagonal forward wall at a distance of 179 cm from the target centre. The two inner rings around the beam line consist of 18×4 $PbWO_4$ crystals, which can sustain higher count rates without limiting the overall detector dead-time. In front of each BaF_2 module or each group of four $PbWO_4$ crystals, a plastic scintillator tile acts as a veto detector for charged particles. The total solid angle coverage of the combined Crystal Ball and TAPS devices is about 97% of 4π. With this set-up approximately 740 hours of data were taken in two run periods during September 2010 and February 2011. The trigger for the data acquisition system was derived only from the total deposited energy in the Crystal Ball exceeding a threshold of approximately 120 MeV. This rather open condition allowed us to study polarised Compton scattering in parallel with π^0 production [34].

3. Data analysis

The differential cross section for π^0 photoproduction with transverse polarised target and unpolarised beam is given by

$$\frac{d\sigma}{d\Omega} = \sigma_0 \left(1 + P_T T \sin\varphi\right) \tag{4}$$

with the unpolarised differential cross section σ_0 and the target polarisation P_T. The angle φ denotes the orientation of the target spin relative to the reaction plane, defined by

$$\hat{z} = \frac{\vec{k}}{|\vec{k}|} \qquad \hat{y} = \frac{\vec{k} \times \vec{q}}{|\vec{k} \times \vec{q}|} \qquad \hat{x} = \hat{y} \times \hat{z} \tag{5}$$

with pion and photon momenta $\vec{q}$ and $\vec{k}$.

The target asymmetry T depends on the y-component of the target polarisation and is defined as

$$T = \frac{1}{P_T |\sin\varphi|} \cdot \frac{\sigma_+ - \sigma_-}{\sigma_+ + \sigma_-}. \tag{6}$$

The orientation in the $\pm y$ direction is given by $\sin\varphi$, and events are considered as negative polarised (σ_-) if $\sin\varphi < 0$, and positive polarised (σ_+) if $\sin\varphi > 0$. The angle φ is determined event-by-event from the difference of the measured azimuthal angle of the pion and the known target spin orientation in the lab frame.

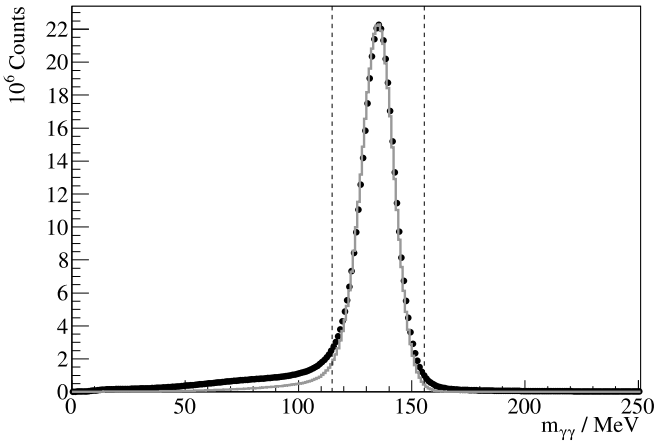

Fig. 1. Invariant $\gamma\gamma$ mass for events with two photons. Data points represent experimental results, while the grey solid line is from a Monte Carlo (MC) simulation of $\gamma p \to p\pi^0$. Dashed vertical lines indicate the accepted range for π^0 masses.

This asymmetry can in principle be measured as a count-rate asymmetry

$$T = \frac{1}{P_T |\sin\varphi|} \cdot \frac{N_+ - N_-}{N_+ + N_-} \tag{7}$$

where $N_\pm$ denote count rates for the two different polarisation states of the target protons rates normalised to the photon flux. Other normalisation factors such as target density, and detection efficiency cancel in the ratio. With a frozen spin butanol target, however, Eq. (7) is no longer sufficient due to background contributions from unpolarised material in the target. In this case, the count rate on butanol decomposes to $N^{\text{but}} = N^p + N^C$ with count rates N^p from free protons, and N^C from other materials. Because the spin 0^+ nuclei ^{12}C and ^{16}O cannot be polarised, N^C does not depend on the target polarisation, and so the measured asymmetry is

$$T^{\text{but}} = \frac{N^p_+ + N^C - N^p_- - N^C}{N^p_+ + N^C + N^p_- + N^C} = \frac{N^p_+ - N^p_-}{N^p_+ + N^p_- + 2N^C}. \tag{8}$$

The numerator of Eq. (8) is intrinsically background free, but the subtraction of N^C in the denominator requires a very precise knowledge and reproduction of different carbon background contributions. These have shown to be very difficult to evaluate quantitatively in the π^0 threshold region because there is a large amount of coherent π^0 production on carbon at energies $\omega \lesssim 250$ MeV. In addition, the recoil proton remains undetected due to its low energy and cannot be used to discriminate background reactions from proton events. Therefore in the present analysis we do not determine the target asymmetry T, but the corresponding polarised cross section

$$\sigma_T = \sigma_0 T = \frac{\sigma_+ - \sigma_-}{P_T |\sin\varphi|}, \tag{9}$$

which can be obtained directly from the count-rate difference $N^{\text{but}}_+ - N^{\text{but}}_-$ for positive and negative target polarisations. The carbon background contributes to both σ_+ and σ_- in the same way and hence cancels in Eq. (9). However, photon flux, target density, and detection efficiencies have to be taken into account.

The π^0 mesons are identified by detecting two photons in coincidence (BR = 98.82%) and their invariant mass $m_{\gamma\gamma}$ is used as the selection criterion. All events with exactly two time-correlated neutral clusters within ±5 ns are considered and their reconstructed invariant mass $m_{\gamma\gamma}$ must fulfil the condition 115 MeV <

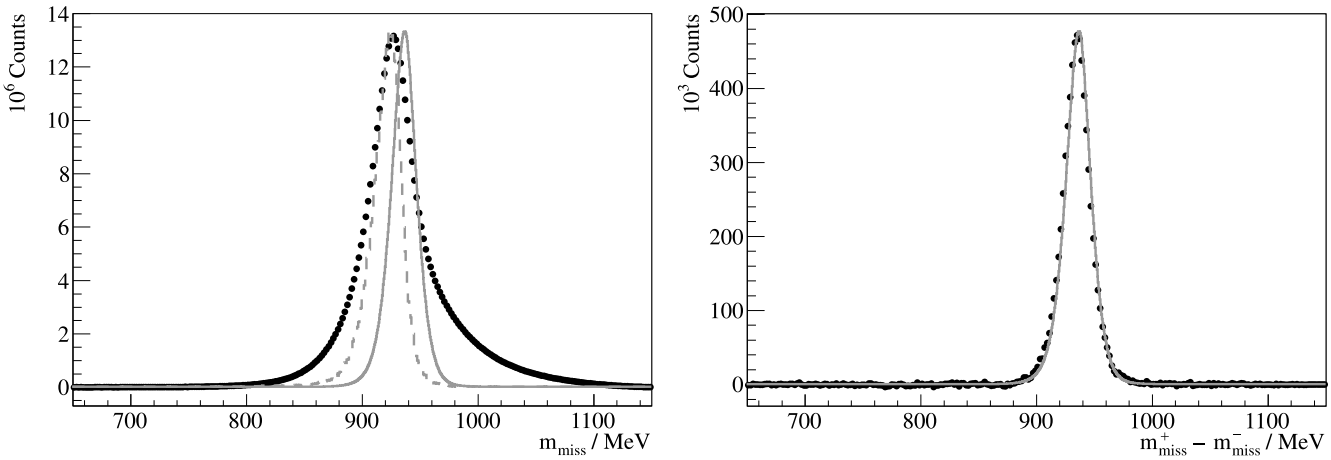

Fig. 2. Left: Missing-mass distribution obtained from butanol target. Data points represent experimental results, while the grey solid and dashed lines are from MC simulations of $\gamma p \to p\pi^0$ and coherent π^0 production on ^{12}C, respectively (not to scale). Right: Polarisation-dependent missing-mass distribution, where unpolarised contributions cancel and only counts from polarised protons remain. Data points represent experimental results, while the grey solid line is from an MC simulation of $\gamma p \to p\pi^0$.

$m_{\gamma\gamma} < 155$ MeV (see Fig. 1). For any accepted photon pair, a kinematic fit constraining $m_{\gamma\gamma}$ to m_{π^0} is performed to reconstruct the π^0 meson with improved energy and angular information. The reconstructed π^0 four-vector is used together with the tagged photon energy information to identify the reaction channel $\gamma p \to p\pi^0$, using the missing mass

$$m^2_{\text{miss}} = (p + k - q)^2 \,, \tag{10}$$

which is evaluated from the four-momenta $p = (m_p, \vec{0})$ of the target proton, $k = (\omega, \vec{k})$ of the beam photon, and $q = (\varepsilon, \vec{q})$ of the reconstructed π^0. For $\gamma p \to p\pi^0$, the missing mass should be equal to the mass of the recoil proton. Here the target particle is explicitly assumed to be a free proton at rest, which is not fulfilled for quasi-free processes on bound nucleons or coherent π^0 production on ^{12}C or ^{16}O (see Fig. 2). Cuts on the missing-mass values are applied for the selection of $\gamma p \to p\pi^0$ events. Central position and width of these cut ranges are chosen energy dependent to give as much discrimination of quasi-free and coherent processes compared to the free proton contributions. To determine these cut ranges, the missing-mass distributions with different spin orientations, m^+_{miss} and m^-_{miss} are subtracted for each energy bin. All unpolarised contributions cancel and only counts from free polarised protons of the butanol target material remain (see Fig. 2 right).

Detector acceptance and reconstruction efficiency are determined from MC simulations of $\gamma p \to p\pi^0$. Reaction kinematics are produced with an event generator based on MAID [35] and DMT [36] model predictions for π^0 photoproduction observables with a polarised target. Generated events are propagated through a GEANT4 simulation of the Crystal Ball / TAPS set-up, folded with detector resolutions and trigger conditions. Both models gave the same result.

The polarised differential cross sections σ_T are determined according to

$$\sigma_T = \sigma_0 T = \frac{1}{P^y_{\text{eff}}} \cdot \frac{N^{\text{but}}_+ - N^{\text{but}}_-}{\varepsilon \cdot \rho_p} \cdot \frac{1}{2\pi \sin\theta}. \tag{11}$$

Where $N^{\text{but}}_\pm$ denote the angular- and energy-dependent count rates normalised to the individual photon flux, ε the reconstruction efficiency, and ρ_p the target proton density. The effective target polarisation P^y_{eff} is calculated on an event-by-event basis from the target polarisation P_T and the relative pion azimuthal angle φ according to

$$P^y_{\text{eff}} = P_T |\sin\varphi|. \tag{12}$$

In order to increase the effective target polarisation, only events with $|\sin\varphi| \geq 0.35$ are accepted for σ_T. This cut, which minimises the relative uncertainty in σ_T, is equivalent to an exclusion of certain ϕ_{π^0} ranges, which reduces the overall acceptance but increases the effective polarisation from about 51% to 62%. The spin-dependent butanol count rates $N^{\text{but}}_\pm$ in Eq. (11) still include background contributions from quasi-free and coherent π^0 production on carbon, which cancel in the determination of σ_T but still contribute to the statistical uncertainties.

Global systematic uncertainties arise from the determination of the photon flux (3%) and the overall detector and electronics performance (3%). For the target density the total uncertainty of 6% is given by the effective target length (2.0 ± 0.1 cm) and the packing fraction ($61\% \pm 2\%$). The target polarisation has been determined with an accuracy of 2%. Quadratic addition of the individual contributions results in global uncertainties for σ_T of about 8%. Furthermore, an energy- and angle-dependent systematic uncertainty is estimated from comparisons to a second independent analysis where asymmetries T have been determined from the butanol data set and additional data from a liquid hydrogen target. This second analysis method has larger statistical errors and was primarily used to evaluate the systematic errors in the experiment. Hydrogen count rates are used in the denominator of the asymmetry definition from Eq. (7), so also with this analysis scheme no subtraction of carbon background events is required. Therefore the target asymmetry T can be determined from

$$T = \frac{1}{P^y_{\text{eff}}} \cdot \frac{N^{\text{but}}_+ - N^{\text{but}}_-}{2N^{\text{H}}} \cdot \frac{\rho^{\text{H}}_p}{\rho^{\text{but}}_p} \tag{13}$$

with the effective degree of polarisation P^y_{eff}, and positive / negative polarisation states for T as described above. N^{H} is the count rate with hydrogen target normalised to the flux and $\rho^{\text{but,H}}_p$ are the target area-densities. The obtained asymmetries T from the cross-check analysis are multiplied with unpolarised cross sections σ_0 from Ref. [1] and the remaining difference between the results from both analyses is attributed as energy and angle dependent systematic uncertainty.

This procedure is demonstrated in Fig. 3, which shows the measured angular distributions at four different energies. The dashed and dashed-dotted lines are two-parameter Legendre fits to the measured data and to the cross-check analysis. The difference is taken as an additional angular-dependent systematic uncertainty.

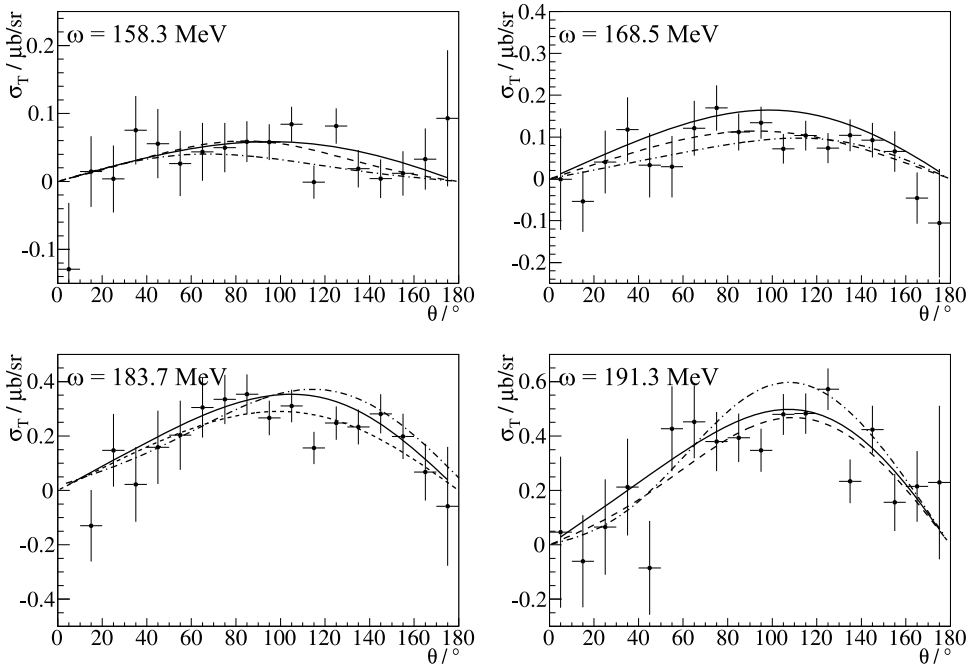

Fig. 3. Polarised differential cross sections σ_T in four selected 1 MeV wide energy bins. The data points represent Crystal Ball / TAPS results with statistical uncertainties only. Solid lines are predictions of the DMT model [36], while dashed and dashed-dotted lines show two-parameter Legendre fits to the experimental data and the cross-check analysis [37], respectively.

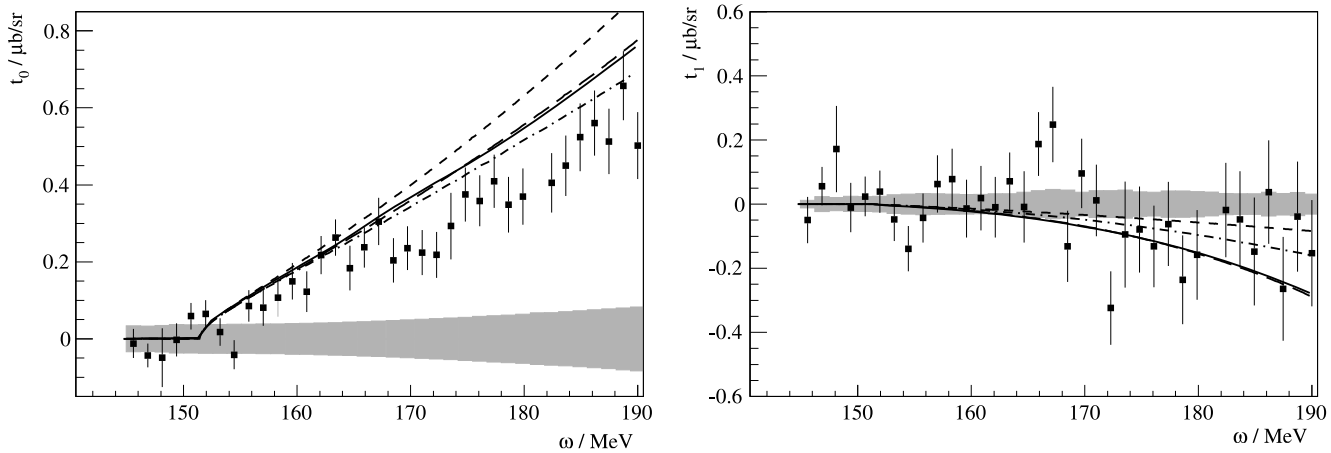

Fig. 4. Legendre coefficients t_n for σ_T. Data points represent experimental results, error bars denote statistical uncertainties, grey shaded bands show absolute systematic uncertainties. The lines show the DMT model prediction [36] (solid), the multipole fit in Ref. [1] using the naïve parametrisation of Eq. (1) with constant $\beta = 3.35 \cdot 10^{-3}/m_{\pi^+}$ (short-dashed), a prediction of Gasparyan, Lutz [38] (long-dashed), and the ChPT4 description in Ref. [8] (dashed-dotted).

4. Experimental results

Differential cross sections σ_T for selected photon energies from π^0 threshold up to $\omega = 190$ MeV are shown in Fig. 3 in comparison to predictions from the DMT model [36]. In addition, cross-section measurements were fitted to a sum of two Legendre polynomials $P_{0,1}(z = \cos\theta)$ according to

$$\sigma_T = \frac{q}{k} \sin\theta \, [t_0 P_0(z) + t_1 P_1(z)] \tag{14}$$

with coefficients $t_{0,1}$ and pion and photon momenta q and k. Such fits allow for a more compact description of the experimental results as well as for an easier comparison between measured cross sections and calculations. In Fig. 3, curves of the Legendre fits show a good agreement with the DMT model calculations. The energy dependence of the Legendre coefficients $t_{0,1}$, which is presented in comparison to different model predictions in Fig. 4, shows that the coefficient t_1 is in agreement with the values predicted by various calculations. The lowest and dominating coefficient t_0 is systematically smaller than the different model predictions within its statistical uncertainties, but still consistent with the model values if the systematic uncertainties are taken into account.

5. Multipole extraction

Our experimental values for σ_T were used in combination with fits on σ_0 and Σ results from Ref. [1] for a single-energy truncated partial-wave analysis up to a given angular momentum order $\ell_{\max}$ to determine electromagnetic multipoles $E_{\ell\pm}$, $M_{\ell\pm}$ as fit parameters. A first extraction of multipoles in the π^0 threshold region was presented in Ref. [1] where data on σ_0 and Σ were used to extract and disentangle the real parts of all four S- and P-wave

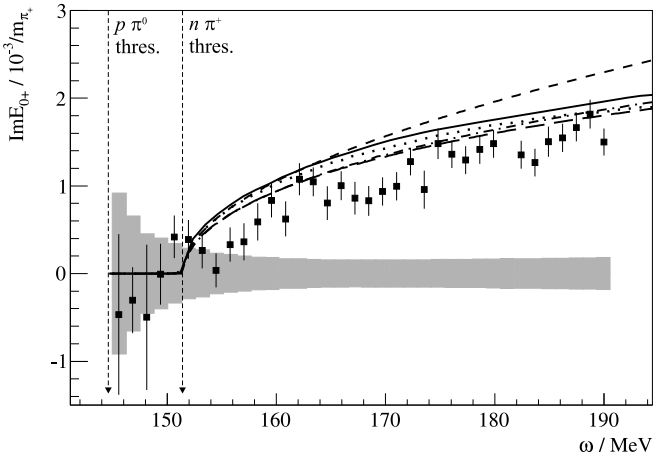

Fig. 5. Imaginary part of E_{0+} from single-energy fits to σ_T. Data points show experimental results with statistical uncertainties (error bars) and absolute systematic uncertainties (grey shaded band). The lines are the DMT model prediction (solid), the naïve parametrisation of Eq. (1) with constant $\beta = 3.35 \cdot 10^{-3}/m_{\pi^+}$ (short-dashed), a prediction of Gasparyan, Lutz [38] (long-dashed), the ChPT4 description in Ref. [8] (dashed-dotted), and a HBChPT4 calculation from Ref. [11] (dotted), scaled by a factor 3.35/2.71 to match the unitary value of β at the $n\pi^+$ threshold.

multipoles (E_{0+} and E_{1+}, M_{1-}, M_{1+}) in the π^0 threshold region. The previous experiment was insensitive to the S-wave imaginary part ImE_{0+}, so only an approximation employing Eq. (1) with constant $\beta = 3.35 \cdot 10^{-3}/m_{\pi^+}$, the unitary value at the $n\pi^+$ threshold, was used. The imaginary parts of P-waves are negligible and become significant only at beam energies above 200 MeV due to the excitation of the $\Delta(1232)$ resonance. D-wave multipoles were calculated in the Born approximation and entered the fits as fixed values, while any higher multipole orders were neglected. The new data for σ_T in this Letter provide access to the imaginary part of E_{0+} and allow for a model-independent determination of S- and P-wave multipoles in the π^0 threshold region (given the applicability of the assumptions of real P- and Born-only D-waves). The data are not sufficiently accurate to determine the small D-wave multipoles directly.

Only our new experimental results for σ_T were directly used for determination of the imaginary part of the E_{0+} multipole. The differential polarised cross section σ_T is given by

$$\sigma_T = \frac{q}{k}\sin\theta\left\{3\mathrm{Im}\left[E_{0+}^*(E_{1+}-M_{1+})\right]+ 3\mathrm{Im}\left[4E_{0+}^*(E_{2+}-M_{2+})- E_{0+}^*(E_{2-}-M_{2-})\right]\cos\theta\right\} \quad (15)$$

for $\ell_{\max} = 2$ and the assumption of real P- and D waves. The real parts of S- and P-wave multipoles were fixed to energy-dependent parametrisations from Ref. [1], imaginary parts of P-waves were assumed to vanish, and D-waves were included as fixed Born terms. The single-energy results for ImE_{0+}, which is the only free fit parameter in this approach, are presented in Fig. 5. Extracted values for ImE_{0+} differ by less than 2% between fits with $\ell_{\max} = 1$ and $\ell_{\max} = 2$, which indicates that D-wave contributions in Eq. 15 are small. We stress again that this is the first direct determination of ImE_{0+} from experimental data. The results clearly confirm the rapid rise above the $n\pi^+$ threshold as expected from the unitary cusp. The data are below the naïve parametrisation of Eq. (1) with constant $\beta = 3.35 \cdot 10^{-3}/m_{\pi^+}$ (short-dashed line in Fig. 5). The difference between this parametrisation and the theoretical curves indicates the sensitivity to the energy dependence of β in Figs. 4 and 5. However, within their uncertainties, the data are not in significant disagreement with model predictions and results from ChPT. A fit with two parameters β_0, β_1 and the relation

$$\beta(\omega) = \beta_0(1+\beta_1 \cdot k_{\pi^+}) \quad \text{with} \quad k_{\pi^+} = \frac{\omega-\omega_{\mathrm{thr}}}{m_{\pi^+}} \quad (16)$$

where $\omega_{\mathrm{thr}} = 151.44$ MeV is the photon energy at the $n\pi^+$ threshold, takes the energy dependence of β into account and yields $\beta_0 = (2.2 \pm 0.2_{\mathrm{stat}} \pm 0.6_{\mathrm{syst}}) \cdot 10^{-3}/m_{\pi^+}$ and $\beta_1 = (0.5 \pm 0.5_{\mathrm{stat}} \pm 0.9_{\mathrm{syst}})$. The systematic uncertainties in $\beta_{0,1}$ were estimated from multipole fits using σ_T data shifted by their respective experimental systematic uncertainties. Various calculations [8,11,36,38] predict a decrease of $\beta(\omega)$ with rising photon energies, corresponding to a negative value for β_1. However, the large uncertainties in the $\beta_{0,1}$ parameters from our fit make clear that a reliable determination of the energy dependence of $\beta(\omega)$ is not possible with our current single-energy results for ImE_{0+}. Consequently, when comparing the imaginary part of E_{0+} to different theory predictions (see Fig. 5), the rather large statistical and systematic uncertainties in ImE_{0+} in the π^0 threshold region do not allow significant conclusions about the differences between theoretical calculations and experimental results to be drawn at this time.

6. Conclusion and outlook

We have presented a first measurement of σ_T for π^0 photoproduction in the near-threshold region. Together with our previous results from [1] we were able to extract all S- and P-wave amplitudes, including the first direct determination of the imaginary part of the E_{0+} multipole from experimental data, in the energy region where ChPT calculations are expected to converge. The imaginary part of E_{0+} confirms the rapid rise above the $n\pi^+$ threshold. Our results for ImE_{0+} are somewhat lower than predicted by unitarity and model calculations, but no significant deviation is observed within the experimental uncertainties. The accuracy of the experimental data is not yet sufficient to determine precise values for the $\beta(\omega)$ parameter and its energy dependence. However, we have demonstrated that this will be possible in future measurements with reduced statistical and systematic uncertainties. Furthermore, by measuring additional spin observables with similar precision, this method of a model-independent multipole analysis can be extended to higher energies where nucleon resonances lead to a more complex partial-wave structure.

Acknowledgements

The authors wish to acknowledge the excellent support of the accelerator group of MAMI. This material is based upon work supported by the Deutsche Forschungsgemeinschaft (SFB 443, SFB 1044), the European Community Research Activity under the FP7 programme (Hadron Physics, Contract No. 227431), Schweizerische Nationalfonds, the U.S. Department of Energy Office of Science, Office of Nuclear Physics, under Award Numbers DE-AC05-06OR23177 and DE-FG02-01ER41194, the U.S. National Science Foundation, the UK Sciences and Technology Facilities Council (STFC 57071/1, 50727/1), the Natural Science and Engineering Research Council (Canada), the Dynasty Foundation, and the MSE Program "Nauka" (Contract No. 825).

References

[1] D. Hornidge, et al., Phys. Rev. Lett. 111 (2013) 062004.
[2] M. Hennebach, et al., Eur. Phys. J. A 50 (2014) 19.
[3] D. Gotta, et al., Hyperfine Interact. 209 (2012) 57.
[4] V. Bernard, U.-G. Meißner, Annu. Rev. Nucl. Part. Sci. 57 (2007) 33.
[5] V. Bernard, Prog. Part. Nucl. Phys. 60 (2008) 82.

[6] A.M. Bernstein, PoS CD12 (2013) 024.
[7] M. Hilt, S. Scherer, L. Tiator, Phys. Rev. C 87 (2013) 045204.
[8] M. Hilt, B.C. Lehnhart, S. Scherer, L. Tiator, Phys. Rev. C 88 (2013) 055207.
[9] C. Fernández-Ramírez, A.M. Bernstein, Phys. Lett. B 724 (2013) 253.
[10] V. Bernard, N. Kaiser, U.-G. Meißner, Phys. Rev. Lett. 74 (1995) 3752.
[11] V. Bernard, N. Kaiser, U.-G. Meißner, Eur. Phys. J. A 11 (2001) 209.
[12] V. Baru, C. Hanhart, M. Hoferichter, B. Kubis, A. Nogga, D.R. Phillips, Nucl. Phys. A 872 (2011) 69.
[13] S. Weinberg, in: Transactions of the N.Y. Academy of Science Series II, vol. 38, 1977, p. 185.
[14] N. Fettes, U.-G. Meißner, Nucl. Phys. A 693 (2001) 693.
[15] N. Fettes, U.-G. Meißner, Phys. Rev. C 63 (2001) 045201.
[16] A.M. Bernstein, M.W. Ahmed, S. Stave, Y.K. Wu, H. Weller, Annu. Rev. Nucl. Part. Sci. 59 (2009) 115.
[17] A.S. Raskin, T. Donnelly, Ann. Phys. (N.Y.) 191 (1989) 78.
[18] D. Drechsel, L. Tiator, J. Phys. G 18 (1992) 449.
[19] C. Fernández-Ramírez, A.M. Bernstein, T.W. Donnelly, Phys. Rev. C 80 (2009) 065201.
[20] M. Watson, Phys. Rev. 95 (1954) 228.
[21] E. Fermi, Suppl. Nuovo Cim. 2 (1955) 17.
[22] A.M. Bernstein, Phys. Lett. B 442 (1998) 20.
[23] B. Ananthanarayann, Phys. Lett. B 391 (2006) 634.
[24] E. Korkmaz, et al., Phys. Rev. Lett. 83 (1999) 3609.
[25] V. Bernard, N. Kaiser, U.-G. Meißner, Phys. Lett. B 383 (1996) 116.
[26] K.-H. Kaiser, et al., Nucl. Instrum. Methods A 593 (2008) 159.
[27] I. Anthony, J.D. Kellie, S.J. Hall, G.J. Miller, J. Ahrens, Nucl. Instrum. Methods A 301 (1991) 230.
[28] J.C. McGeorge, et al., Eur. Phys. J. A 37 (2008) 129.
[29] A. Thomas, Eur. Phys. J. Spec. Top. 198 (2011) 171.
[30] C.S. Akonadi, et al., Phys. Rev. Lett. 113 (2014) 102001.
[31] C. Rohlof, H. Dutz, Nucl. Instrum. Methods A 526 (2004) 126.
[32] R. Novotny, IEEE Trans. Nucl. Sci. 38 (1991) 379.
[33] A.R. Gabler, et al., Nucl. Instrum. Methods A 346 (1994) 168.
[34] P.P. Martel, R. Miskimen, et al., Phys. Rev. Lett. 114 (2015) 112501.
[35] D. Drechsel, S.S. Kamalov, L. Tiator, Eur. Phys. J. A 34 (2007) 69.
[36] S.S. Kamalov, S.N. Yang, D. Drechsel, L. Tiator, Phys. Rev. C 64 (2001) 032201.
[37] P.B. Otte, Ph.D. thesis, Johannes Gutenberg-Universität Mainz, 2015.
[38] A. Gasparyan, M.F.M. Lutz, Nucl. Phys. A 848 (2010) 126.